IOPscience iopscience.iop.org

Home Search Collections Journals About Contact us My IOPscience

Damage of silicate glasses during stress corrosion

This article has been downloaded from IOPscience. Please scroll down to see the full text article.

2011 J. Phys.: Conf. Ser. 319 012005

(http://iopscience.iop.org/1742-6596/319/1/012005)

View the table of contents for this issue, or go to the journal homepage for more

Download details:
IP Address: 134.157.76.34
The article was downloaded on 21/11/2011 at 11:40

Please note that terms and conditions apply.

Journal of Physics: Conference Series **319** (2011) 012005 doi:10.1088/1742-6596/319/1/012005

Damage of silicate glasses during stress corrosion

F. Lechenault
[1] CEA-Saclay, IRAMIS, SPEC, F-91191 Gif-sur-Yvette, France
[2] LCVN, UMR 5587 CNRS-UM2, Place Eugène Bataillon, 34095 Montpellier Cedex 5, France

C. L. Rountree
CEA-Saclay, IRAMIS, SPCSI, F-91191 Gif-sur-Yvette, France

F. Cousin
CEA-Saclay, IRAMIS, Laboratoire Léon Brillouin, CNRS UMR12, F-91191 Gif-sur-Yvette, France

J.-P. Bouchaud
Science and Finance, Capital Fund Management, 6 Boulevard Haussmann, 75009 Paris, France

L. Ponson
Institut Jean Le Rond d'Alembert, UMR 7190, CNRS and Univ. Paris 06 UPMC, 75005 Paris, France

E. Bouchaud
CEA-Saclay, IRAMIS, SPEC, F-91191 Gif-sur-Yvette, France

E-mail: elisabeth.bouchaud@cea.fr

Abstract. We show that water penetrates into the silicate glass matrix during stress corrosion fracture by probing what is stored under the fracture surface using neutron reflection. The concentration profile determined for two different values of the external loading exhibits a region close to the fracture surface where the water content is fairly elevated, suggesting a high amount of damage.

1. Introduction

Although glass is the archetype of brittle elastic materials, it was shown by S. Wiederhorn that most of the mechanical energy released is not spent in the creation of free surfacess [1]. As a matter of fact, the measured fracture energies were shown to be seven to ten times larger than expected, and the nature of the "lost energy" has been since then the topic of passionate discussions [2, 3, 4, 5]. The first possibility one may think of as an origin to the observed discrepany between measured and expected energies is plasticity. However, although plastic deformation − a local densification − as high as $\sim 20\%$ can be observed when silicate glasses undergo shear or pressure or both [6], like under the tip of an indenter [7], such a contribution is

Published under licence by IOP Publishing Ltd

not likely to arise at the tip of a crack submitted to mode I tension. As a matter of fact, it can be shown that the expected size of the plastic zone is of a few nanometers at most, so that the energy dissipated through plasticity is much smaller than the energy spent in surface creation.

It has also been suggested, first from Molecular Dynamics (MD) simulations [8, 9, 10, 11, 12] that energy dissipation might be due to the occurrence of "quasi-brittle" damage [13, 14, 15, 16]. Quasi-brittle damage is observed in very disordered materials such as wood [17, 18, 19], mortar or concrete [20, 21], which have negligible plasticity. In a perfect crystal, where atomic bond orientations and energies are δ-distributed, bonds at the crack tip will break first because stress concentration is maximum there. In contrast, because of disorder, the bonds which break first are likely to be at some distance from the one sitting exactly at the crack tip. As a result, small cracks nucleate, and subsequently grow in a zone ahead of the crack tip often referred to as the "Process Zone" (PZ), the extent of which depends on the location of the most brittle parts of the inhomogeneous specimen. For the materials quoted above, the PZ size may be of macroscopic dimensions. Does this effect arise in glass too, albeit at a much smaller scale? Glass is known to be quite homogeneous down to length scales of $\sim$10 nm. Hence, the nature of the disorder which might be at the origin of such quasi-brittleness is not completely clear. However, one can suggest that the local orientation of Si-O bonds with respect to the external applied stress may play an important role. In this case, the amorphous structure providing local random orientations, it can be a source of disorder sufficient to nucleate and grow damage at a distance from the crack tip. Indications of such damage can be seen on the fracture surfaces of metallic glasses [22, 23].

Direct observations of the mechanisms involved in the fracture of silicate glasses are more challenging, because of the very small length scales involved. Furthermore, following a dynamic crack during its propagation is inaccessible experimentally. Actually, in order to follow crack growth with an Atomic Force Microscope (AFM), with a scan size of $\sim$ 100nm, taking on the order of one minute to acquire, the crack velocity cannot exceed $\sim$ 1nm.s^{-1}. Depending on the degree of humidity, stress corrosion subcritical cracks in silicate glasses can progress at very slow velocities, i.e. typically 10^{-12} to 10^{-5}m.s^{-1} under very moderate external tensile stresses, thanks to a chemical reaction involving the water molecules in the surrounding environment. This is a complex phenomenon, which started to be studied in the sixties [24, 25] and is not yet fully understood (see [26] for a recent review).

In the classical picture, proposed first by Michalske and Bunker [27], water molecules break the Si-O bonds located exactly at the crack tip thanks to a hydrolysis reaction. For small enough external loads, the crack velocity is controlled by the rate of the chemical reaction, which depends both on the degree of ambient humidity and on the applied stress. This regime is traditionally referred to as "Stage I" [24, 28]. At higher applied loads, when the crack velocity reaches a value that depends on humidity, the slowest phenomenon (which imposes its kinetics to the crack velocity) is the diffusion of water molecules to the tip along the fracture surfaces. Since surface diffusion is not sensitive to the external applied load, the crack velocity in this "Stage II" does not depend on it either.

This classical picture, however, does not take into account the disordered character of the glass structure, while in glass, the complex arrangement of chemical bonds make the occurrence of disjunctions away from the tip most probable, which results in "quasi-brittle" [28, 16] damage. *In situ* Atomic Force Microscopy (AFM) experiments [2, 4, 29] were performed in order to follow a stage I stress corrosion crack during its propagation,and crack openings ahead of the main tip were claimed to be observed. These observations, however, are still very controversial [3, 30]. Because AFM observations are restricted to the free surface of the specimens, several artifacts can alter the measurements [5, 31]. And, as a matter of fact, there are several significant differences between the free surface and the bulk of the specimen. Of particular importance is the exposure to water in the case of stress corrosion fracture: while the free surface is in direct contact

with the ambient humidity, water molecules have to diffuse within the material for Si-O bonds to break at a distance from the crack tip. Although experiments have been performed at high temperature only [32, 33], a rough extrapolation of Tomozawa et al's results [34] suggests a water diffusion coefficient in silica of the order of $\sim 10^{-21}\mathrm{cm}^2.\mathrm{s}^{-1}$ at room temperature. This means that the penetration length of water molecules into unstrained glass should be approximately 3pm (respectively 0.3Å) during the time it takes for a crack moving at $10^{-6}\mathrm{m.s}^{-1}$ (respectively at $10^{-8}\mathrm{m.s}^{-1}$) to cover 100μm.

However, because of the huge stresses concentrated at the crack tip, diffusion is enhanced by orders of magnitude in the vicinity of the tip during fracture [35, 36], as observed both in glass [37] and in several other materials [38, 39]. Therefore, water can penetrate into the glass and spread within a small zone around the crack tip. Because of the heterogeneity of the material mentioned above, water breaks bonds and creates microcracks ahead of the crack tip. This in turn increases further the diffusion of water, thereby creating more corrosion and potentially leading to a substantial damaged zone. Alternatively, and as suggested by recent experiments [40], water penetration can result in a volumic expansion of the zone saturated with water ahead of the crack, leading to effective cohesive forces that oppose the crack motion. This mechanism is similar to toughening by phase transformation in some ceramics, and does not require material deformation beyond its yield stress [41]. In both scenarii, a rather thick layer of water should remain trapped underneath the nominal fracture surface after the crack has propagated and stresses are relaxed. Since the diffusion constant is so small in unloaded silica glass (more than 100 days for travelling 1 nm), one should observe post-mortem a "fossil" water profile, essentially frozen-in at the time of its creation, with a thickness on the order of the size of the damaged zone. The aim of this work is to provide quantitative evidence for the above scenario using neutron reflectivity [42, 43] to measure the thickness of the water layer left behind the crack. We find that the penetration depth of water is on the order of a hundred ångströms, with a rather large volumic concentration in the vicinity of the free surface (of the order of 50%). This suggests that diffusion has been accompanied by a chemical degredation of the glass network. This observation strongly supports that the abnormally high fracture energy of silica glass results from stress corrosion damage within a nanometric volume surrounding the crack tip.

2. Fracture experiments

Fracture experiments were conducted in a highly controlled manner via Double Cleavage Drilled Compression (DCDC) samples. In this geometry, the stress at the crack tip naturally decreases, enabling us to conduct all our experiments in the sub-critical stress corrosion regime. DCDC samples used herein are cuboids of size 5 x 5 x $25\mathrm{mm}^3$ with a 1mm diameter hole drilled in the center. They are made of Corning 7980 pure silica. The fracture experiments were conducted in a glove box which had been saturated either with light or with heavy water. Two symmetrical precracks are first initiated from the hole of the sample as described in [4] (Fig. 1a). Subsequently the load is adjusted in order to reach a desired velocity [4]. Sample 1, broken in light water environment was submitted to an inital load of 1970N corresponding to a stress intensity factor K_I of $0.32\mathrm{MPa.m}^{1/2}$ (average velocity of $2.3^{-10}\mathrm{m.s}^{-1}$). For the sample 2, broken in a heavy water environment, Zone 1 (Fig. 2c) corresponds to a stress intensity factor K_I=$0.61\mathrm{MPa.m}^{1/2}$. Zone 2 (Fig. 2c) corresponds to a stress intensity factor K_I=$0.77\mathrm{MPa.m}^{1/2}$ (average velocity of $4.10^{-6}\mathrm{m.s}^{-1}$).

Note that heavy water has a coherent length density $b_w = 6.39\,10^{-6}\text{Å}^{-2}$ higher than the one of silica ($b_s = 3.41\,10^{-6}\text{Å}^{-2}$), and of opposite sign to that of light water ($b_l = -0.53\,10^{-6}\text{Å}^{-2}$). If some water is trapped in the vicinity of the surface of the sample, the reflectivity of the sample should thus increase in the presence of heavy water (sample 2) whereas it would only weakly decrease with light water (sample 1).

Figure 1. Fracture experiment. (a) Scheme of the DCDC sample submitted to uniaxial compression. Two symmetric cracks progress under local mode I tension from the cylindrical hole drilled in the middle of the specimen. (b) Picture of the actual experiment. A strength gauge and a displacement gauge allow for the measurement of force and displacement during the experiment.

3. Neutron reflection experiments

Specular Neutron Reflectivity (SNR) measurements have been carried out on the horizontal time-of-flight EROS reflectometer (LLB, Saclay, France) with a fixed angle θ of 1.195, with a neutron white beam covering wavelengths λ from 4Å to 25Å, covering an accessible q-range (scattering wavevector $q = 2\pi \sin\theta/\lambda$) from 0.005 Å^{-1} to 0.032Å^{-1}.

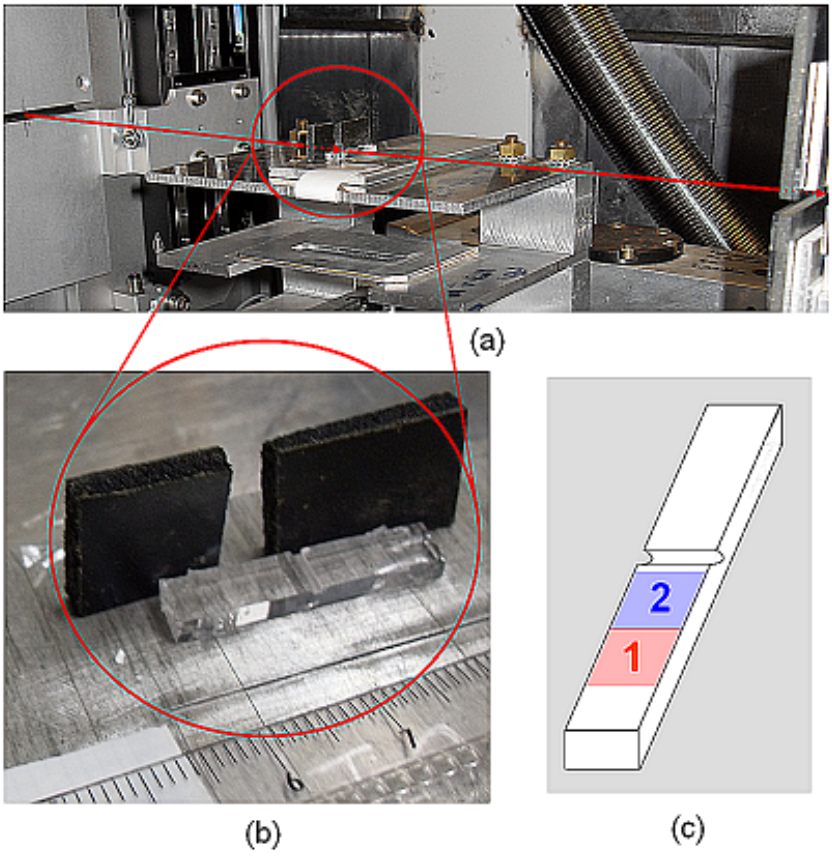

Figure 2. (a) Picture of the experimental setup. The neutron beam is schematized in red, incoming from the last slit of the collimator, reflecting on the sample and going within the slit in front of the detector. (b) Picture of the broken sample, showing the two black sheets of B_4C used to select one area of interest (see text). (c) Sketch of the broken sample, with the two parts described in the text.

In order to select Zone 1 or Zone 2 (see Fig. 2c)) in sample 2 described above, we used the following trick. The sample was almost completely hidden on the neutrons path by two black sheets of B_4C, a strong neutron absorber, to let the neutrons illuminate only the desired region (Fig. 2 a and b). In order to test that the selected region was flat enough to allow a correct measurement, we have checked that the full width at half max of the alignment rocking curve was lower than 0.25°. When this was not the case, the illuminated region was reduced until

this condition was met. The resulting illuminated surfaces were very small, from $\sim 10\text{mm}^2$ to $\sim 25\text{mm}^2$. Because of this smallness, we used very long counting times to get a reasonable noise-to-signal ratio, up to 48 hours per illuminated region. In particular, we measured the background independently from the sample with high precision, enabling its subtraction with a good accuracy.

4. Results

Fig. 3 shows also that the reflectivity of the control specimen corresponds perfectly to the Fresnel reflectivity $R_F = (q - \sqrt{(q^2 - q_c^2)})^2/(q + \sqrt{(q^2 - q_c^2)})^2$ of a semi-infinite silica diopter for which the coherent length density is equal to b_s. The onset of total reflection is given by $q = q_c = \sqrt{4\pi b_s}$, where $b_s = 3.41\,10^{-6}\text{Å}^{-2}$ is the value found in the literature [43, 44].

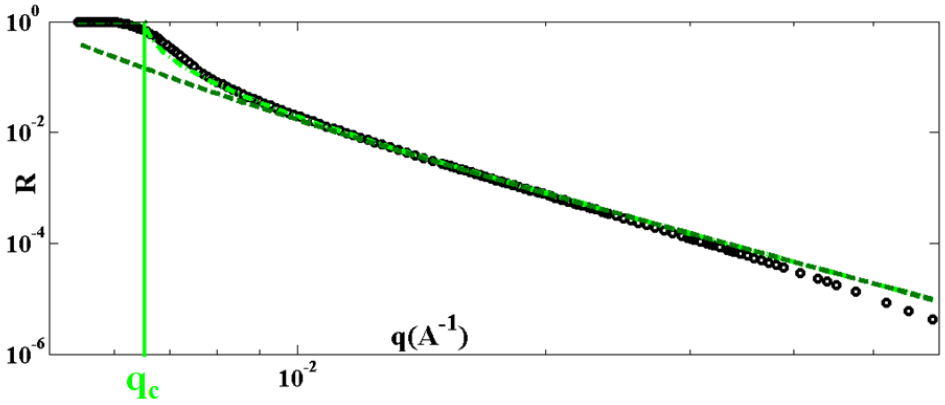

Figure 3. Experimental neutron reflectiviy of the control sample plotted as a function of the scattering wavevector q (open black circles). The theoretical Fresnel reflectivity (green dashed-dotted line) $R_F = (q - \sqrt{(q^2 - q_c^2)})^2/(q + \sqrt{(q^2 - q_c^2)})^2$ superimposes very well to the experimental curve up to $q \simeq 4.10^{-2}\text{Å}^{-1}$. The total reflectivity plateau takes place for $q < q_c$ with $q_c = \sqrt{4\pi b_s}$. The 2^{nd} order Born approximation used for a slab of pure silica is plotted in dotted dark green, and it can be seen that it fits very nicely both the experiment and the theoretical expression as soon as $q > 9.10^{-3}\text{Å}^{-1}$, i.e. for $R \leq$some 10^{-2}.

While Fig. 4 shows that the reflectivity is unchanged when fracture is achieved in a light water environment, Fig. 5 shows a huge increase in the reflectivity of samples broken in a heavy water environment when compared to the reflectivity of the unbroken control specimen.

5. Theoretical analysis of the experimental observations

While the experimental curve presented in Fig. 4 does not show any measurable effect, the curves presented in Fig. 5 clearly show a huge change in the reflectivity of broken samples when compared to the reflectivity of the unbroken control specimen. Since the roughness of the fracture surfaces is larger than the roughness of the control specimen, one should *a priori* expect a decrease of the reflectivity of the broken samples. The difference seen in Fig. 5 is therefore underestimated.

In order to fit the neutron reflectivities measured in Zones 1 and 2 (Fig. 5), we have used a second order Born approximation, assuming that the heavy water concentration is not a constant, but that it decreases with the distance z from the free surface of the tested sample as $\phi(z)$. This concentration profile translates into a coherent length density profile $b_w(z) = b_w\phi(z)$. Since most of the workable signal is obtained in a region of large scattering vectors q, far enough from total reflexion, reflectivities are quite small, and hence the reference situation is the free case, when all the incident neutrons are transmitted.

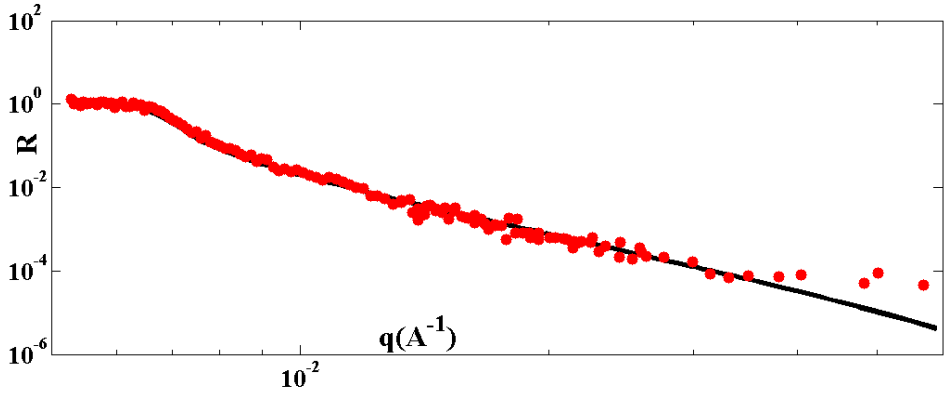

Figure 4. Experimental neutron reflectiviy of the light water stress corrosion fracture surface (red dots) compared to the measured Fresnel reflectivity (plain black line) of the control sample.

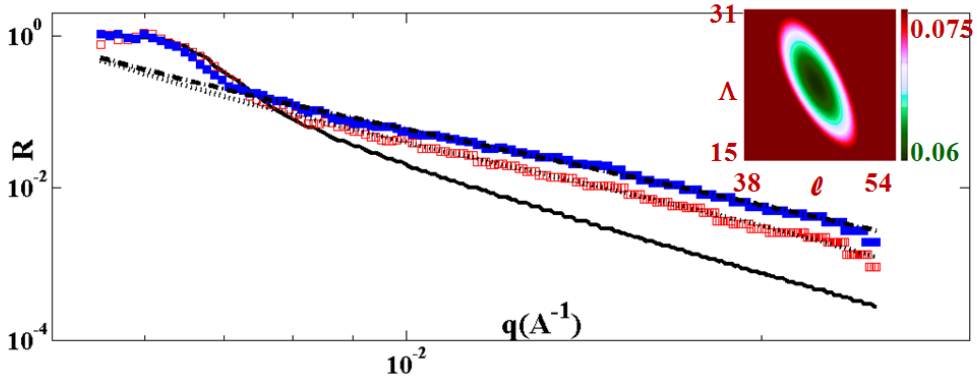

Figure 5. Experimental neutron reflectivities plotted as a function of the scattering wavevector q for: the control sample (plain black line),and for Zones 1 and 2 on the fracture surface of the specimen broken in a heavy water environment, corresponding respectively to stress intensity factors $K_I = 0.61\text{MPa.m}^{1/2}$ (empty red squares) and $K_I = 0.77\text{MPa.m}^{1/2}$ (full blue squares). The experimental results corresponding to Zone 1 and Zone 2 are fitted using Eqs. (10), (12) and (13). Fits are respectively a dotted black line and a black dashed line. The best fits correspond to $\phi_0^I = 0.348 \pm 0.003$, $\ell^I \approx 43$Å and $\Lambda^I \approx 35$Å in Zone 1, and $\phi_0^{II} = 0.567 \pm 0.003$, $\ell^{II} \approx 46$Å and $\Lambda^{II} \approx 23$Å in Zone 2. Inset: Contour lines of the fit root-mean square error in the plane (ℓ, Λ) in Zone 2, showing that while the combination $\ell_{eff} = \Lambda + \ell$ is rather well pinned down by the fit, $\Lambda - \ell$ is a "soft" direction. The relative experimental rms error per point is 0.075, whereas the minimum relative error achieved by the fit is 0.06.

The neutron wave function ψ obeys the following eigenvalue equation:

$$\frac{d^2\psi(z)}{dz^2} + (q^2 - V(z))\psi(z) = 0 \tag{1}$$

with $V(z) = 4\pi(b_s + b_w\phi(z))$ a small perturbation: $V(z) \ll q^2$.

We write:

$$\psi = \psi_0 + \psi_1 + \psi_2 + ... \tag{2}$$

with ψ_1 and ψ_2 the first and second order corrections (in V).

Adapting the calculation of [45], one finds:

$$\psi_{n+1}(z) = \int_0^\infty dz' V(z')\psi_n(z')G_0(z, z') \tag{3}$$

where the Green function $G_0(z, z' > 0)$ relevant for our boundary conditions refers to the free case:

$$\begin{array}{ll} G_0(z,z') = -\frac{1}{2iq}\exp\left(-iq(z'-z)\right) & \text{if } z<0 \\ G_0(z,z') = -\frac{1}{2iq}\exp\left(-iq|z'-z|\right) & \text{if } z>0 \end{array} \tag{4}$$

Hence:

$$\psi_1(z) = \frac{i}{2q}[\int_0^z dz' V(z') \exp -iqz + \int_z^\infty dz' V(z') \exp -2iqz' \exp iqz] \tag{5}$$

and:

$$\psi_2(z) = \int_0^\infty dz' V(z') \psi_1(z') G_0(z', z) \tag{6}$$

with $z' > 0$ and $z < 0$, i.e.:

$$\psi_2(z) = \frac{i}{2q}\int_0^\infty dz' V(z') \psi_1(z') \exp\left(-iq(z'-z)\right) \tag{7}$$

Adding the first and second order contributions, we get the total wave vector perturbation:

$$\begin{aligned} \psi_1(z) + \psi_2(z) \quad = \quad & \left(\frac{i}{2q}\int_0^\infty dz' V(z') \exp -2iqz'\right) \exp iqz \\ & -\frac{1}{4q^2}\int_0^\infty dz' V(z') [\exp -2iqz' \\ & \int_0^{z'} dz'' V(z'') + \int_{z'}^\infty dz'' V(z'') \exp -2iqz''] \exp iqz \end{aligned} \tag{8}$$

Using the above expression, we get the expression of the reflectance r to order V^2:

$$\begin{aligned} r \quad & = \frac{i}{2q}\int_0^\infty dz' V(z') e^{-2iqz'} - \frac{1}{4q^2}\int_0^\infty dz' V(z') \times \\ \times \quad & \left[e^{-2iqz'}\int_0^{z'} dz'' V(z'') + \int_{z'}^\infty dz'' V(z'') e^{-2iqz''}\right] \end{aligned} \tag{9}$$

The reflectivity R is $R = |r|^2$. In order to check the validity of our second order Born approximation, we first verify that our result in Eq. (9) tends to the Fresnel reflectivity for high values of q when V is a constant equal to $q_c^2 = 4\pi b_s$. This limit leads to the following reflectivity:

$$R = r_0^2 = \frac{q_c^4}{16q^4}\left(1 + \frac{q_c^2}{2q^2}\right)^2 + O(\frac{q_c^8}{q^8}) \tag{10}$$

which coincides with the corresponding large q expansion of the Fresnel reflectivity (see Fig. 3).

We then tried to fit the reflectivities in Zones 1 and 2 (Fig. 5) using the simplest function involving a single length scale, i.e. $\phi(z) = \phi_0 \exp\left(-z/\Lambda\right)$. Although this can be made to fit the Zone 1 results, the reflectivity increase in Zone 2 is too large to be accounted for using this simple function. Hence, guided by the idea that there might be a saturated layer of depth ℓ close to the surface that becomes more diffuse deeper in the sample, we posit that:

$$\begin{array}{ll} \phi_w(z) = \phi_0 & \text{if } z < \ell \\ \phi_w(z) = \phi_0 \exp\left(-(z-\ell)/\Lambda\right) & \text{if } z > \ell \end{array} \tag{11}$$

This choice leads to a reflectance r that can be written as: $r = r_0 + r_1 + r_2$, with r_0 as the Fresnel reflectance (Eq. (10)) and:

$$r_1 = -\frac{2\pi b_w \phi_0}{q(2iq\Lambda + 1)} \exp(-2iq\ell) \tag{12}$$

$$\begin{aligned} r_2 &= -\frac{4\pi^2 (b_w\phi_0)^2}{q^2} \left[\frac{1}{2q^2} [\exp(-2iq\ell)(1 + 2iq\ell) - 1] \right. \\ &+ \left. \frac{\Lambda \exp(-2iq\ell)}{(2iq\Lambda + 1)(iq\Lambda + 1)} (\Lambda + 2\ell + 2iq\Lambda\ell) \right] \end{aligned} \tag{13}$$

Fig. 5 shows the best fits of the experimental measurements performed on the two fracture surfaces using Eqs. (10), (12) and (13):

$$R = |r_0 + r_1 + r_2|^2 \tag{14}$$

The best fit is achieved with $\phi_0^I = 0.348 \pm 0.003$, $\ell^I \approx 43$Å and $\Lambda^I \approx 35$Å in (slow) Zone 1, while in (fast) Zone 2, $\phi_0^{II} = 0.567 \pm 0.003$, $\ell^{II} \approx 46$Å and $\Lambda^{II} \approx 23$Å. Note that ϕ_0 is very accurately determined by the fit, although the error bar we quote only accounts for statistical uncertainty, and not systematic effects coming from the choice of the fitting function and of the interval over which the data is fitted. On the other hand, the quality of fit has a "soft direction" in the plane (ℓ, Λ), as represented in the inset of Fig. 5. As expected, the total effective width of the layer, $\ell_{eff} = \ell + \Lambda$ is better determined than ℓ and Λ separately. The statistical error bar on ℓ_{eff} is smaller than 1Å, but again systematic errors are much larger. As shown in the inset of Fig. 5, ℓ_{eff} can be varied by $\sim \pm 5$Å and still lead to an acceptable fit.

In order to evaluate the change in reflectivity due to the presence of light water under the fracture surface, we have computed R using Eq. (14), assuming that $\ell \simeq 46$ Åis not very much with K_I, and $\Lambda \simeq 90$Å, since the penetration depth seems to increase when the external load is decreased. Because b_l is not only negative but approximately ten times smaller in absolute value than b_w, the reflectivity loss does not depend much on the amount of water stored under the surface, i.e. it does not depend much on ϕ_0. We have chosen to compute R in Eq. (14) for two values of ϕ_0, 0.05 and 0.5. The two results are actually indistinguishable in Fig. 6 (green dots). This means that our method is restricted to the use of heavy water as a corrosive agent.

Figure 6. Expected reflectivity (green dots) using Eq. (14) for light water, assuming a concentration profile of the type described by Eqs. (11), with ϕ_0, 0.05 and 0.5, $\ell \simeq 46$ Åand $\Lambda \simeq 90$ Å. The solid black line is the reflectivity of the control specimen, and the open red circles correspond to the measurements for sample 1, broken in a light water environment.

6. Discussion

Our results [46] clearly show that heavy water is present over $\sim$ 65 to 85Å under the stress corrosion fracture surface of pure silica in the conditions of our experiments. This penetration depth is much larger than what is expected using a room temperature extrapolation of the diffusion coefficient of light water in silica [34] (to our knowledge, there are no such results concerning heavy water, for which diffusion should be even smaller). The heavy water concentration within the first 40-50 Å under the fracture surface is found to be very high (35 and 57%) - it actually seems to be larger for a larger value of the applied load -. These values

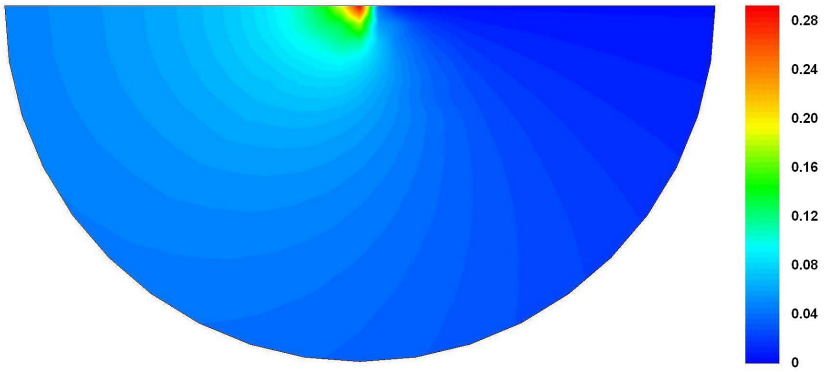

Figure 7. Finite element simulations of the dilation field $D(x,y) = \epsilon_{xx}(x,y) + \epsilon_{yy}(x,y)$ in the vicinity of the crack tip in the mid-plane of the specimen for an external loading $K_I = 0.61$ MPa.m$^{1/2}$. The crack propagates from right to left, and the color code indicates the amplitude of $D(x,y)$.

are too high to account for a situation where there would be no mechanical damage within the silica network. The resulting decrease of the concentration of silica may not have a negligible effect on the change of reflectivity, but it has not been taken into account in our interpretation of the data.

A likely explanation of our observations is as follows: diffusion enhancement in the vicinity of the crack tip, where huge tensile stresses are present ([39], [35], [47]), allows the water to penetrate inside the bulk and create a damaged zone which helps water progressing further still. Our neutron scattering experiment gives information about the water penetration depth in the direction perpendicular to the fracture surface. To investigate how far water penetrates parallel to the crack propagation direction, one would need a detailed self-consistent model for the coupled growth of the damaged zone and the diffusion of water. We grossly simplify the problem by computing the dilation field $D(x,y) = \epsilon_{xx}(x,y) + \epsilon_{yy}(x,y)$ in the vicinity of the crack tip within a purely elastic model, and postulating that the water penetrates in a region defined by $D(x,y) > D_c$, and infer the anisotropy of the water penetration from that of the iso-dilation lines. We analyze DCDC samples identical to those used in the experiments and compute the dilation field in the mid-plane of the specimen using finite element simulations, with element sizes decreasing exponentially as approaching the crack tip, so that the strain field is resolved at the nanometer scale within that region. As shown in Fig. 3 for an external loading $K_I = 0.61$ MPa.m$^{1/2}$, the domain at the crack tip with a high level of dilation extends deeper in the direction of propagation than in the perpedicular direction, by a factor $\sqrt{2}$. This result is consistent with the predictions of Linear Elastic Fracture Mechanics in the limit of very small distances from the crack tip [28]. Therefore, we estimate that water penetrates roughly $9-12$nm ahead of the crack tip, in the crack propagation direction. If one identifies the water-rich region with a damaged zone, our estimate is in agreement with the fact that the strain field observed in the vicinity of a stress corrosion crack tip is elastic only on scales larger than ~ 10nm [48].

We observe an increase of the neutron reflectivity, not only with respect to the Fresnel case, but also with respect to the case where we assume a heavy water single-length scale, exponentially decreasing profile. This has prompted us to postulate the presence of an homogeneous layer of water, followed by an exponentially decaying profile. The width of the layer, $\ell \approx 4$nm, is significantly larger than the height fluctuations on silica fracture surfaces which do not exceed 1nm [49, 50]. It is tempting to interpret this zone as a strongly damaged zone, with a density of microcracks that is larger when the stress intensity factor – and the crack velocity – is higher. This would naturally explain why $\phi_0^{II} > \phi_0^I$, although we have no clear explanation as why

$\ell^I \approx \ell^{II}$. This might be due to the cancellation of two opposite effects: a stronger stress enhances the diffusion of water in the bulk, but at the same time the crack speed is larger, leaving less time for the corrosion mechanism to operate. The latter mechanism in fact explains why the exponential region, which is probably more sensitive to diffusion, is wider in Zone 1 than in Zone 2 ($\Lambda^I > \Lambda^{II}$). In order to be more quantitative, one requires at this stage a detailed model for the formation of the damaged zone, dynamically coupled to the water profile. A more systematic study of the effect of the external applied stress on the heavy water content would be needed to provide a sound basis for such a quantitative model. Further experiments will be performed with larger specimens such as to increase the intensity of the reflected neutron beam.

Preliminary results have been obtained recently [51] using a Finite Element model which takes into account both the enhancement of water diffusion and damage formation in the vicinity of the crack tip: a concentration profile composed of a very damaged zone saturated in water followed by a rapid decrease of the water content was obtained, as well as an exponential dependence of the crack velocity with the applied stress intensity factor.

Acknowledgments

Part of this work was supported by ANR CORCOSIL. We acknowledge very interesting discussions with S. Chapuliot.

References

[1] Wiederhorn S 1969 *J. of the Am. Ceram. Soc.* **52** 99–105
[2] Célarié F, Prades S, Bonamy D, Ferrero L, Bouchaud E, Guillot C and Marlière C 2003 *Phys. Rev. Lett.* **90** 075504
[3] Guin J P and Wiederhorn S M 2004 *Phys. Rev. Lett.* **92** 215502
[4] Prades S, Bonamy D, Dalmas D, Bouchaud E and Guillot C 2004 *Int. J. of Sol. and Struct.* **42** 637–645
[5] Fett T, Rizz G, Creek D, Wagner S, Guin J P, López-Cepero J M and Wiederhorn S M 2008 *Phys. Rev. B* **77** 174110
[6] Rountree C L, Vandembroucq D, Talamali M, Bouchaud E and Roux S 2009 *Phys. Rev. Lett.* **102** 195501
[7] Kermouche G, Barthel E and Vandembroucq D 2008 *Acta Mater.* **56** 3222–3228
[8] Nakano A, Kalia R K and Vashishta P 1995 *Phys. Rev. Lett.* **75** 3138–3141
[9] Kalia R, Nakano A and Vashishta P 1997 *Phys. Rev. Lett.* **78** 689–692
[10] Rountree C L, Kalia R, Lidorikis E, Nakano A, Brutzel L V and Vashishta P 2002 *Annual Review of Materials Research* **32** 377–400
[11] Kalia R, Nakano A, Vashishta P and Rountree C 2003 *IEEE Computer Society* 36–39
[12] Rountree C L, Prades S, Bonamy D, Bouchaud E, Kalia R and Guillot C 2007 *J. of Alloys and Compounds* **434-435** 60–63
[13] Bažant Z and Cedolin L 1991 *Stability of Structures: Elastic, Inelastic, Fracture and Damage Theories* (Oxford University Press, New-York, USA)
[14] Bažant Z 1997 *Int. J. of Fract.* **83** 19–40
[15] Morel S 2007 *Int. J. of Sol. and Struct.* **44** 42724290
[16] Bonamy D and Bouchaud E 2011 *Physics Reports* **498** 1–44
[17] Morel S, Bouchaud E, Schmittbuhl J and Valentin G 2002 *Int. J. of Fract.* **114** 307–325
[18] S Morel E B and Valentin G 2002 *Phys. Rev. B* **64 (104101)** 1–8
[19] Morel S, Dourado N, Valentin G and Morais J 2005 *Int. J. of Fract.* **131** 385–400
[20] Bažant Z 2002 *Eng. Fract. Mech.* **69** 165–205
[21] Mourot G, Morel S, Bouchaud E and Valentin G 2005 *Phys. Rev. E* **71** 016136
[22] Xi X K, Zhao D Q, Pan M X, Wang W H, Wu Y and Lewandowski J J 2005 *Phys. Rev. Lett.* **94** 125510
[23] Bouchaud E, Boivin D, Pouchou J L, Bonamy D, Poon B and Ravichandran G 2008 *Europhys. Lett.* **83** 66006
[24] Wiederhorn S M 1968 *Int. J. of Fract. Mech.* **4** 171–177
[25] Wiederhorn S M 1969 *J. Am. Ceram. Soc.* **52**
[26] Ciccotti M 2009 *J. Phys. D: Appl. Phys.* **42, Special Issue "Fracture: from the atomic to the geophysical sclae", Guest Editors E. Bouchaud and P. Soukiassian** 214006
[27] Michalske T and Bunker B 1984 *J. Appl. Phys.* **56** 2686–2693
[28] Lawn B 1993 *Fracture of Brittle Solids- Second Edition* (Cambridge University Press)

[29] Rountree C L, Prades S, Bonamy D, Bouchaud E, Kalia R and Guillot C 2010 *Phys. and Chem. of Glasses-Europ. J. of Glass Sci. and Tech. Part B* **51** 127–132
[30] Lòpez-Cepero J, Wiederhorn S, Fett T and Guin J P 2007 *Int. J. Mater. Res.* **98** 1170–1176
[31] Lechenault F, Pallares G, George M, Rountree C, Bouchaud E and Ciccotti M 2010 *Phys. Rev. Lett.* **104** 025502
[32] Davis K and Tomozawa M 1996 *J. of Non-Cryst. Sol.* **201** 177–198
[33] Berger S and Tomozawa M 2003 *J. of Non-Cryst. Sol.* **324** 256–263
[34] Tomozawa M and Davis K M 1999 *Mat. Sci. and Eng. A* **272** 114119
[35] Larché F and Voorhees P 1996 *Defect and Diffusion Forum* **129-130** 31–36
[36] Greer A 1996 *Defects and Diffusion Forum* **129-130** 163–180
[37] Tomozawa M, Han W and Lanford W A 1991 *J. Am. Cer. Soc.* **74** 2573
[38] Aziz M J, Zhao Y, Gossmann H J, Mitha S, Smith S P and Schiferl D 2006 *Phys. Rev. B* **73** 054101
[39] Guery J, Baudry J, Weitz D A, Chaikin P M and Bibette J 2009 *Phys. Rev. E* **79** 060402(R)
[40] Wiederhorn S Private communication
[41] Kelly P M and Rose L R F 2002 *Prog. Mat. Sci.* **47** 463–557
[42] Bouchaud E, Farnoux B, Sun X, Daoud M and Jannink G 1986 *Europhys. Lett.* **2** 315–322
[43] Cousin F and Menelle A *La réflectivité de neutrons* (Les Editions du CNRS)
[44] http://wwwsfnassofr/Enseignement/Outils/Table/indexhtml
[45] Charmet J C and de Gennes P G 1983 *J. Opt. Soc. Am.* **73** 1777–1784
[46] Lechenault F, Rountree C L, Cousin F, Bouchaud J P, Ponson L and Bouchaud E 2011 *Phys. Rev. Lett.* **106** 165504
[47] Nazarov A V and Mikheev A A 2008 *J. Phys.: Condens. Matter* **20** 485203
[48] Pallares G 2010 *Analyse multi-échelle des mécanismes de propagation de fissure dans les verres d'oxydes* Ph.D. thesis Montpellier II University (France)
[49] Bonamy D, Ponson L, Prades S, Bouchaud E and Guillot C 2006 *Phys. Rev. Lett.* **97** 135504
[50] Ponson L 2007 *Annales de Phys.* **32** 1
[51] Chapuliot S and Bouchaud E Preliminary results